RSC Advances

RSC Advances

www.rsc.org/advances

ROYAL SOCIETY OF CHEMISTRY

www.rsc.org/advances

Binding studies of aristololactam- β-D-glucoside and daunomycin to human serum albumin

Abhi Das and Gopinatha Suresh Kumar*

Biophysical Chemistry Laboratory, Chemistry Division
CSIR-Indian Institute of Chemical Biology
Kolkata 700 032

Running Title: aristololactam-β-D-glucoside and daunomycin-HSA interaction.

Address for Correspondence

Dr. G. Suresh Kumar, Ph.D

Senior PrincipalScientist, Biophysical Chemistry Laboratory

CSIR-Indian Institute of Chemical Biology

4, Raja S.C. Mullick Road, Kolkata 700 032

India

Phone: +91 33 2472 4049/2499 5723

Fax : +91 33 2472 3967

e.mail: gskumar@iicb.res.in/gsk.iicb@gmail.com

_____

*Author to whom all correspondence may be addressed.

Abstract

The interaction of the plant alkaloid aristololactam-β-D-glucoside (ADG) and the anticancer agent daunomycin (DAN) with human serum albumin (HSA) was investigated. Absorption and steady-state fluorescence spectroscopy, steady state fluorescence anisotropy, circular dichroism and isothermal titration calorimetry techniques have been exploited to characterize the binding phenomena. Absorbance and fluorescence quenching experiments revealed the formation of a strong complex of DAN and HSA, and comparatively weaker complex between ADG and HSA. Spectroscopic analysis suggested binding affinity of ADG to HSA to be of the order of 10^4 M^{-1} and that of DAN-HSA to be of the order of 10^5 M^{-1}. Fluorescence quenching data suggested a static quenching mechanism in both the cases at the ground state. Three dimensional fluorescence and circular dichroism data are consistent with a conformational change in the protein on binding of ADG and DAN. Calorimetric study revealed exothermic binding of both drugs which was favored by negative standard molar enthalpy and standard molar entropy contributions. ADG was found to be a weaker binder to HSA compared to DAN. Detailed comparative biophysical aspects of the binding are presented.

Keywords: Aristololactam-β-D-glucoside; daunomycin; human serum albumin; binding; thermodynamics.

Introduction

Human serum albumin is the most abundant plasma protein which acts as a major contributor to colloid osmotic pressure of plasma. It functions primarily as a carrier protein for steroids, fatty acids and thyroid hormones, and plays a role in stabilizing extracellular fluid volume. HSA binds to a wide variety of drugs and plays an important role in their pharmacology and pharmacodynamics. From X-ray crystallographic studies it has been established that HSA is a helical monomeric protein of molecular weight 66 kDa having three homologous domains (I–III), each of which is comprises A and B subdomains.[1,2] At physiological pH HSA assumes the normal form (N). The two major drug/small molecule binding sites on HSA are located in the hydrophobic cavities in subdomains IIA and IIIA which are designated as sites I and II, respectively.[1,2] Drug-HSA interactions can provide information on drug storage, control of drug delivery to tissue receptors and prevention of the drug from being rapidly metabolized. Consequently, a large number of studies on the interaction of small molecules and drugs to HSA have been recently undertaken particularly on the structural aspects.[3-8] Effectiveness of these small molecules as therapeutic agents may depend on their binding ability. Therefore, insights into the architecture and specificity of small drugs binding on HSA may be an essential factor in protein based therapeutic drug design.

Aristololactam-β-D-glucoside (Fig. 1A), a phenanthrenic lactam derivative extracted from *Aristolochia indica*, is of extensive biological and biogenetic interest for its prospective clinical and pharmacological uses.[9,10] Aristololactam- β-D-glucoside has

some structural similarity to daunomycin (Fig. 1B), the widely used chemotherapeutic agent, in that both compounds have conjugated aromatic chromophore with an attached sugar moiety. The sugar moiety may have influence on their clinical utility. Both aristololactam-β-D-glucoside and daunomycin are known to bind strongly to DNA by intercalation and, inhibit DNA and RNA synthesis.[9-17]

The binding aspects of aristololactam-β-D-glucoside and daunomycin to DNA and RNA have been extensively characterized.[11-25] However, their binding to serum albumins is not well studied. From previous investigations using fluorescence quenching and resonant mirror biosenser experiments the interaction of daunomycin with serum albumin has been evidenced.[26,27] The binding of daunomycin to HSA was also mapped by molecular modeling studies.[27] The thermodynamic characterization of the binding of daunomycin to HSA by calorimetric techniques, however, has not yet been reported. Again, the binding studies of aristololactam-β-D-glucoside to serum proteins remain totally unexplored. Therefore, in this paper we compared the molecular aspects of the binding of aristololactam-β-D-glucoside and daunomycin to human serum albumin. A complete structural and thermodynamic study from a variety of biophysical experiments is presented.

Results and discussions

Absorption spectral study of the interaction

The interaction of ADG and DAN (drugs hereafter) with HSA was monitored at first by absorption spectroscopy. Both ADG and DAN have characteristic visible absorption spectra in the 300–600 nm region (Fig. 2) with band maxima around 398 nm and 480 nm, respectively, that were monitored to understand the interaction process. Results of absorption spectral titration of constant concentration of ADG and DAN with increasing concentrations of HSA are presented in Fig. 2A and B. Binding of both drugs to HSA resulted in hypochromic effect in absorbance at the λ_{max}. At P/D (protein/drug molar ratio) 100, the absorbance of ADG at the 398 nm decreased by about 22% from that of the free drug absorabance. In the case of DAN at the saturating P/D of 30, the hypochromic effect was ~ 20%. The presence of isosbestic points at 418 nm for ADG and 546 nm for DAN indicated equilibrium between the free and bound drugs. The spectral data were analyzed by Benesi-Hildebrand plot[28] to determine the equilibrium constant using the equation

$$\frac{1}{\Delta A} = \frac{1}{\Delta A_{max}} + \frac{1}{K_{BH}(\Delta A_{max})} \times \frac{1}{[M]} \qquad (1)$$

The binding constants evaluated yielded K_{BH} values of 3.22×10^4 and 1.04×10^5 M^{-1} for ADG and DAN, respectively. A binding affinity value for the DAN-HSA interaction very close to that obtained here was reported by Zou and colleagues from the results of resonant mirror biosensor technique.[27]

Fluorescence spectral study

HSA contains only one Trp at 214 in the subdomain IIA. The binding of the drugs to the protein may affect the fluorescence of the Trp residues depending on the alteration of the surrounding microenvironment. The fluorescence of the protein

was therefore monitored to understand the effect of ADG and DAN binding. In the presence of both ADG and DAN the intrinsic fluorescence spectrum of HSA was remarkably quenched. Steady state fluorescence spectral changes of HSA in the presence of increasing concentrations of ADG and DAN are presented in Fig. 3A and B. The quenching mechanism was analysed by the traditional Stern–Volmer equations.[29] A plot of F_o/F versus [Q] (Fig. 3C and D) was linear in both the cases indicating the occurrence of only one type of quenching. The K_{sv} values elucidated from these plots for ADG and DAN binding at 298.15 K were 3.10×10^4 and 2.24×10^5 M^{-1}, respectively. The quenching phenomena are usually classified as dynamic or static, characterised by their dependence on temperature and viscosity. Dynamic quenching occurs when the fluorophore and the quencher come into contact during the lifetime of the excited state. Static quenching, on the other hand, occurs on fluorophore-quencher complex formation in the ground state. Differentiation of these is possible from temperature dependent data. So we performed temperature dependent studies at three different temperatures viz. 288.15, 298.15 and 308.15 K, respectively. The values of K_{sv} at these temperatures are depicted in Table 1. It can be seen that the K_{sv} values for both ADG and DAN complexation decreased with increasing temperature. This suggests that the quenching followed a static mechanism and was due to complex formation, which undergoes dissociation on increasing temperature and the dynamic collision effects, if any, may be considered to be negligible. It is noted that previous study of Zou and colleagues have suggested static quenching mechanism in the fluorescence quenching of HSA by

DAN.[27] The quenching data was also analyzed by the Lineweaver–Burk equation[30] where from the static quenching constant (K_{LB}) was obtained as the ratio of the intercept to slope of the Lineweaver–Burk plot, describing the efficiency of quenching at the ground state. The data on the temperature dependent fluorescence studies of ADG and DAN-HSA complexations are presented in Table 1. The decreasing trend in the magnitude of the K_{LB} values with increasing temperature was in accordance with the temperature dependence of the K_{sv} values and is consistent with a static quenching mechanism.

Conformational study by circular dichroism spectroscopy

From CD spectral data the secondary structure of HSA was found to contain about 55% α-helix, 27% β-sheet and 16-17% random coiled structures, respectively, which is in full agreement with the literature reports.[31] Upon complexation with DAN the conformational change induced in HSA led to a reduction of 14.6% of α-helical structure (Fig. 4A). The unfolding and loss of helical stability in HSA was caused by secondary structural change induced by DAN. The far-UV spectral changes of HSA with ADG could not be recorded because of the presence of DMSO in the buffer.

The near UV CD spectrum of HSA shows two minima around 262 and 290 nm, characteristic of the disulfide and aromatic chromophores and reflecting the tertiary structural organization of the protein.[32,33] With gradual increase in the concentration of ADG and DAN, the ellipticity of both bands was decreased (Fig. 4B and C), which clearly indicated perturbation of the tertiary structure leading to unfolding of the

native conformation of HSA. However on complexation no induced optical activity was observed for the drugs.

Three-dimensional fluorescence spectroscopy

To understand the conformational changes in a protein upon interaction 3D fluorescence spectra were recorded. The representative 3D fluorescence spectra and the contour maps of HSA in the absence and in the presence of the drugs are presented in Fig. 5 and the corresponding parameters are listed in Table 2. In the figure, peak 'a' and peak 'b' arise due to first order Rayleigh scattering ($\lambda_{ex} = \lambda_{em}$) and second order Rayleigh scattering peak ($\lambda_{ex} = 2\lambda_{em}$), respectively.[31] ADG and DAN interaction led to decrease of the fluorescence intensity of HSA at peak 'a' because the scattering effect was weakened by formation of the complex. Peak 1 (λ_{ex} = 280 nm, λ_{ex} = 350 nm) is the characteristic fluorescence spectral behaviour of Trp and Try residues. On binding of the drugs to HSA it was observed that the fluorescence intensity of peak 1 decreased. In the case of ADG-HSA binding, Stokes shift increased where as Stokes shift decreased in DAN-HSA binding which supports the change in polarity and hydrophobicity around the Trp residue. Peak 2, another strong fluorescence peak (λ_{ex}= 230 nm, λ_{em} = 350 nm) was obtained due to the π-π* transition of the polypeptide backbone of the protein. Changes in fluorescence property of this peak are associated with the change in the conformation of the polypeptide backbone or the environment of the polypeptide. Fluorescence intensity of peak 2 also decreased significantly on binding of ADG to

HSA. All these data revealed that binding of both ADG and DAN induced some unfolding in the polypeptide chain of HSA.

Steady-state fluorescence anisotropy study

Anisotropy is essentially used as a probe to assess the flexibility or tumbling of small ligands on binding to biomacromolecules. Anisotropy may provide information about size, shape, and segmental flexibility of a fluorophore's environment.[34] Increase in the rigidity of the environment surrounding the fluorophore results in an increase in the fluorescence anisotropy. Monitoring the anisotropy can thus help in understanding the location of molecular interactions in heterogeneous environments like proteins, DNA, RNA etc. Figure 6A and B reveals a marked increase in fluorescence anisotropy of free drug molecules with the presence of increasing concentration of HSA. The steady-state anisotropy (r) value of free ADG was determined to be ~0.02 which increased to 0.20 after complexation. In the case of DAN, the steady-state anisotropy (r) value increased from 0.03 to 0.24 after binding. These results suggest that the fluorophore drug molecules on binding to HSA have been trapped within a motionally restricted environment of HSA. Effect of urea induced unfolding of protein on anisotropy was also observed. Upon addition of urea on HSA bound drugs, the reverse trend i.e., a steady decrease in the fluorescence anisotropy was observed (Inset: Fig. 6A and B). With increasing concentration of urea entrapped ADG and DAN molecules were apparently released due to denaturation of the protein which leads to the decrease of fluorescence anisotropy of the drug molecules.

Isothermal titration calorimetry

Isothermal titration calorimetry is an effective and sensitive tool to characterize the binding of small molecules to biomacromolecules.[35,36] The ITC profiles for the binding of ADG and DAN to HSA are presented in Fig. 7A and B. Each of the heat burst spikes in the figure corresponds to a single injection of the HSA solution from the syringe into the drug solution in the calorimeter cell. These data were corrected by the corresponding dilution heats derived from the titration of identical amounts of HSA into the buffer alone. The resulting corrected heats, plotted as a function of molar ratio, is depicted in the lower panels. The ITC profiles were monophasic and exothermic in nature in both cases. Exothermic binding of DAN to HSA was suggested from thermodynamic parameters estimated from temperature dependence of the binding constants.[27] The data points in the lower panels reflect the experimental injection heats while the solid lines reflect the calculated fits of the data. All the data were fitted to a single set of identical sites model yielding the binding constant (K), binding stoichiometry (N) and enthalpy (ΔH^o) changes. The standard molar Gibbs energy of the reaction (ΔG^o) and the standard molar entropy contribution ($T\Delta S^o$) were calculated. The binding constant of ADG to HSA at 25 ℃ was evaluated to be 3.50×10^4 M^{-1} with a stoichiometry value 1.25. A ΔH^o value of -2.80 kcal/mol, $T\Delta S^o$ value of 3.44 kcal/mol and ΔG^o -6.24 kcal/mol, respectively, were obtained for the binding. The binding affinity of DAN to HSA was found to be one order higher. For DAN-HSA complexation the K value obtained was 1.95×10^5 M^{-1} with a stoichiometry value 1.13, a ΔH^o value of -3.40 kcal/mol, $T\Delta S^o$ of 3.81

kcal/mol and ΔG^o -7.22 kcal/mol, respectively. The energetics of both the interactions was favored by negative enthalpy and positive entropy changes. The results with DAN is similar to those reported by Zou from temperature dependent resonant mirror biosenser experiments.[27] The binding stoichiometry confirms a 1:1 binding for ADG and DAN-HSA complexation. Variation of the standard molar enthalpy change with temperature can provide information on the heat capacity changes (ΔC_p^o) of the binding. For this the temperature dependence of the binding of ADG and DAN to HSA was studied by performing ITC experiments at three temperatures, viz. 288.15, 298.15 and 308.15 K (Fig. 8A and B). As the temperature increased the binding affinity values for both ADG and DAN decreased and the standard molar enthalpy values increased (Table 3). Variation in the thermodynamic parameters with temperature is depicted in Fig. 9A and B. The negative enthalpy of binding at all the temperatures indicated favorable exothermic binding of the alkaloid and DAN with HSA. From the plots of the variation of the ΔH^0 with temperature, the heat capacity change was deduced to be around -86 and -127 cal/(mol K), respectively, for ADG and DAN binding to HSA. The negative values of ΔC_p^o suggest that the binding is specific and accompanied by burial of non polar surface area.[37] Furthermore, a linear relationship of the enthalpy change with $T\Delta S^o$ with the value of slopes near unity indicates a complete enthalpy-entropy compensation of binding Gibbs energy in both the cases. An enthalpy-entropy compensation behaviour was suggested for DAN-HSA interaction previously.[27]

Different types of forces like hydrophobic, van der Waals interaction, electrostatic, etc. may be involved in protein-ligand interaction. Previous study on DAN-HSA interaction has suggested the involvement of electrostatic interactions as inferred from the pH dependence of the binding, along with strong hydrophobic and hydrogen bond ineractions.[27] DAN has a positive charge on the protonated amino sugar, but ADG is a neutral molecule. To understand the role of polyelectrolytic forces in the complexation, the salt dependence of the binding reaction was studied by performing ITC experiments at three different Na+ concentrations 10 mM, 20 mM and 50 mM Na^+. The thermodynamic parameters evaluated from this study are presented in Table 4. The binding affinity of both ADG and DAN with HSA decreased as the salt concentration increased from 10 mM to 50 mM. From the dependence of K on $[Na^+]$ the observed $\Delta G°$ values were partitioned into two components namely the polyelectrolytic ($\Delta G°_{pe}$) and the non-polyelectrolytic contribution ($\Delta G°_t$) for the binding of ADG and DAN to HSA. These contributions at any given $[Na^+]$ may be calculated from the equations $\partial\log(K)/ \partial\log([Na^+]) = -Z\varphi$, $\Delta G°_{pe} = -Z\varphi\ RT\ln[Na^+]$ and $\Delta G° = (\Delta G°_{pe} +\Delta G°_t)$.[38] The values of $\Delta G°_t$ and $\Delta G°_{pe}$ for the binding of ADG and DAN with HSA at the three $[Na^+]$ are presented in Table 4. The parsing of the Gibbs energy showed that the polyelectrolyte contribution to the binding free energy was significantly smaller in both cases (12% for ADG and 20% for DAN at 10 mM [Na+]) compared to the non-polyelectrolytic contribution but the same was higher for DAU compared to ADG. A pictorial representation of the parsing of the Gibbs energy at three salt concentrations is shown in Fig. 10. The

major contribution to the binding Gibbs energy, therefore, comes in both cases from forces other than the electrostatic interactions. The results confirm the role of electrostatic interaction in DAN-HSA complexation.[27]

Differential scanning calorimetry of ADG and DAN–HSA interaction

Thermal stability of HSA may change upon binding with ligands. The effect of ADG and DAN on the thermal stability of HSA was investigated by using differential scanning calorimetry technique. HSA unfolds cooperatively with a single endothermic peak with melting temperatures of 329.15 K (Fig. 11). Binding DAN induces instability to the protein and the melting temperature decreased to 326.15 K. The melting temperature of ADG-HSA complex, however, remained almost unchanged around 328.15 K. Decrease of the melting temperature of 3K by DAN suggested that the binding destabilized the protein structure while ADG induced no such instability.

Comparison to other alkaloids binding to HSA

A large number of small molecule drugs and natural alkaloids are now known to bind to HSA and most of them bind with affinity in the range 10^4-10^5 M^{-1}. In the context of developing ADG as a potential drug it is perhaps pertinent to compare the binding aspects with that of some natural alkaloids of potential therapeutic utility reported in the literature. Sanguinarine, the benzophenanthridine alkaloid binds to HSA. The nucleic acid binding charged iminium form was found to bind with affinity five times lower than that of the neutral alkanolamine form that had no affinity to nucleic acids.[39] The binding affinity of ADG is even lower than that of the

alkanolamine form. The isoquinoline alkaloids berberine, palmatine and coralyne also binds to HSA more stronger than ADG.[31,40] So the strong binding to nucleic acids and a weaker binding to HSA may be beneficial for the effective delivery of ADG in nucleic acid targeted drug therapy.

Conclusions

The alkaloid ADG has potential drug value and hence its interaction with serum albumin may be important for delivering to different physiological targets in therapeutic applications. ADG was found to have a lower binding affinity towards HSA compared to DAN. This suggests that it could be effectively delivered at required sites with high affinity. The DNA binding of ADG was however higher than that to HSA. The binding of the both drugs induced strong structural perturbation in the protein structure. Both DAN and ADG were trapped and motionally restricted inside the protein cavity. Thermodynamic results showed that the binding was favored by both negative enthalpy and positive entropy changes. Both enthalpy and entropy contributed significantly to the total binding Gibbs energy. Negative heat capacity is correlated to the involvement of significant hydrophobic forces in the complexation. Although the exact binding site of ADG on HSA is still unknown, this study demonstrates that the differential structural features of the sugar molecules, inter alia, appears to contribute significantly to the differences in the binding affinity of these two drugs to serum albumin. The results may be important for employing ADG as a therapeutic agent.

Experimental section

Materials

Human serum albumin (0.99 mass fraction purity, essentially fatty acid and globulin free) and daunomycin hydrochloride (>90% pure) were purchased from Sigma–Aldrich Corporation (St. Louis, MO, USA). Aristololactam-β-D-glucoside (Fig. 1) was extracted from *Aristolochia indica* and crystallized twice from ethanol, and its purity was checked by various physicochemical techniques as reported earlier.[21,23] The stock solution of ADG was prepared in 100% DMSO. HSA, ADG and DAN concentrations were determined spectrophotometrically using molar absorption coefficients of 36,600 M^{-1} cm^{-1} at 280 nm for HSA, 10,930 M^{-1} cm^{-1} at 398 nm for ADG and 11,500 M^{-1} cm^{-1} at 480 nm for DAN, respectively.[23] No deviation from Beer's law was observed in the concentration range used in this study. Deionised and triple distilled water was used for preparing buffer solutions. All experiments were conducted using citrate-phosphate (CP) buffer (10 mM [Na^+]) of pH 7.2, containing 5 mM Na_2HPO_4. Additional 240 mM DMSO was present in the buffer in experiments with ADG. The pH was adjusted using citric acid. pH measurements were made on a Sartorius PB-11 high precision bench pH meter (Sartorius GmBH, Germany) with an accuracy of >±0.01. All other chemicals used were of analytical grade and obtained from Sigma-Aldrich. The buffer solution was filtered through Millipore filters (Millipore India Pvt. Ltd, Bangalore, India) of 0.22 µm pore size.

UV-vis absorbption spectroscopy

Absorbance spectral measurements were performed on a Jasco V660 spectrophotometer (Jasco International Co., Ltd., Hachioji, Japan) in 1 cm path length

matched quartz cuvettes at 25±1 ^{o}C as described earlier.[41,42] Temperature of the cuvette holder was controlled by Peltier controlled devise.

Fluorescence spectroscopy

Steady state fluorescence spectra were measured on a Shimadzu RF-5301PC spectrofluorimeter (Shimadzu Corporation, Kyoto, Japan) at 25±1 ^{o}C following the previously standardised methods of our laboratory.[43] For measurement of intrinsic fluorescence of HSA in the presence of ADG, the protein sample was excited at 295 nm, the excitation maximum of tryptophan, and emission spectra scanned from 300 to 400 nm. Temperature dependent fluorescence spectral studies were conducted on a Hitachi F4010 unit (Hitachi Ltd., Tokyo, Japan) equipped with a Eyela Uni cool water bath (Tokyo Rikakikai Co., Tokyo, Japan) for controlling the sample temperature. The temperature was monitored by the electronic devise Sensortek, model BAT-12 (Sensortek Inc., NJ, USA).

Steady-state anisotropy measurements were carried out at 25±1 ^{o}C using Hitachi F4010 unit (Hitachi Ltd., Tokyo, Japan) spectrofluorimeter. The steady-state anisotropy (r) is defined as

$$r = \frac{(I_{VV} - G.I_{VH})}{(I_{VV} + 2G.I_{VH})} \qquad (2)$$

in which I_{VV} and I_{VH} are the emission intensities when the excitation polarizer is vertically oriented and the emission polarizer is oriented vertically and horizontally, respectively. G is the correction factor defined as

$$G = \frac{I_{HV}}{I_{HH}} \qquad (3)$$

where the intensities I_{HV} and I_{HH} refer to vertical and horizontal positions of the emission polarizer, with the excitation polarizer being horizontal.

Three-dimensional spectroscopy

Three-dimensional (3D) fluorescence spectroscopy experiments were performed at 25 ± 1 ^{o}C on a PerkinElmer LS55 fluorescence spectrometer (PerkinElmer Inc., USA). The fluorescence emission spectra of HSA were measured in the range of 200–500 nm with an increment of 10 nm, the initial excitation wavelength was set at 200 nm and continued up to 340 nm, i.e. the number of scans was 15.

Circular dichroism spectroscopy

A Jasco J815 spectropolarimeter (Jasco International Co., Ltd.,) equipped with a peltier cuvette holder and temperature controller PFD425 L/15 was used for monitoring the conformational changes in the protein on alkaloid binding. The protein concentration and path length of the cuvette used were 1.0 μM and 1 cm, respectively, for near UV CD measurement. The instrument parameters for CD measurements were scan speed of 50 nm/min., bandwidth of 1.0 nm, and sensitivity of 100 milli degrees. Five scans were performed, averaged to improve the signal-to-noise ratio, and smoothed within permissible limits with the Jasco software. The molar ellipticity values in the region of intrinsic CD were expressed in terms of the mean residue molar ellipticity [θ], in units of deg cm^2 $dmol^{-1}$. All the measurements were made at at 25 ± 1 ^{o}C.

Isothermal titration calorimetry

Isothermal titration calorimetry (ITC) experiments were performed with a VP-ITC unit (MicroCal LLC, Northampton, MA, USA) using previously described methods.[44] HSA and drug solutions were degassed on the MicroCal's Thermovac unit before loading to avoid the formation of bubbles in the calorimeter cell. The instrument control, titration and data analysis were automatically performed through the dedicated Origin 7.0 software of the unit. The experiments were carried out as follows. Briefly, aliquots of degassed HSA solution were injected from the rotating syringe (611 rpm) into the isothermal sample chamber containing the drug solutions (1.4235 mL). Each injection generated a heat burst curve (microcalories per second versus time). The area under each heat burst curve was determined by integration using the Origin 7.0 software (MicroCal) to give the measure of the heat associated with that injection. The heat associated with each HSA-buffer mixing was subtracted from the corresponding heat associated with the HSA injection to drug to give the heat of drug-HSA binding. The resulting corrected injection heats were plotted as a function of molar ratio (drug/HSA) and fitted with a model of one set of binding sites and analyzed using the Origin 7.0 software to provide the binding affinity (K), the binding stoichiometry (N), and the standard molar enthalpy of complex formation (ΔH^o). The binding standard molar Gibbs energy change (ΔG^o) values and the standard molar entropy contribution to the binding ($T\Delta S^o$) were calculated according to the standard relations

$$\Delta G^o = -RT\ln K \qquad (4)$$

and

REVISED MANUSCRIPT RA-ART-05-2014-004327

$\Delta G^o = \Delta H^o - T\Delta S^o$ (5)

(where T is the absolute temperature in kelvins and R is the gas constant (1.9872 cal mol^{-1} K^{-1}).

The calorimeter was periodically calibrated electrically and verified with water–water dilution experiments as per the criteria of the manufacturer that the mean energy per injection was <1.30 μcal and standard deviation was <0.015 μcal. In temperature dependent ITC experiments no variation in the buffer pH was observed in the temperature range studied here.

Differential scanning calorimetry

Temperature dependent transition of proteins can be investigated by differential scanning calorimetry (DSC).[42] To study the change in thermal stability of protein upon complexation with the drugs, excess heat capacity as a function of temperature was measured in a MicroCal VP-differential scanning calorimeter (MicroCal LLC). Initially both the cells were loaded with buffer solution, equilibrated at 303.15 K for 15 min. and scanned from 303.15 to 373.15 K at a scan rate of 50 K/ h. The buffer scans were repeated till the base line was reproducible. Typically about 10 to 12 scans were required to obtain a stable base line. On the cooling cycle the sample cell was rinsed and loaded with HSA and then with the drug-HSA complexes. Each experiment was repeated twice with separate fillings. The DSC thermograms of excess heat capacity versus temperature were analysed using the Origin 7.0 software provided with the unit.

Acknowledgements

References

1　D. C. Carter, J. X. Ho, *Adv. Protein Chem.*, 1994, **45**, 153–203.

2　G. Sudlow, D. J. Birkett, D. N. Wade, *Mol. Pharmacol.,* 1976, **12**, 1052–1061.

3　L. Perry, T. Christensen, M. R. Goldsmith, E. J. Toone, D. N. Beratan, J. D. Simon, *J. Phys. Chem. B*, 2003, **107**, 7884–7888.

4　G. Zhang, B. Keita, C. T. Craescu, S. Miron, P. D. Oliveria, L. Nadjo, *J. Phys. Chem. B*, 2007, **111**, 11253–11259.

5　A. Chakraborty, A. Mallick, B. Halder, P. Das, N. Chattopadhyay, *Biomacromolecules*, 2007, **8**, 920–927.

6　Y. J. Hu, Y. Liu, X. H. Xiao, *Biomacromolecules*, 2009, **10**, 517–521.

7　A. Varshney, P. Sen, E. Ahmed, M. Rehan, N. Subbarao, R. H. Khan, *Chirality*, 2010, **22**, 77–87.

8　N. Ibrahim, H. Ibrahim, S. Kim, J. P. Nallet, F. Nepveu, *Biomacromolecules*, 2010, **11**, 3341–3351.

9   Z. Chen, D. Zhu, *The Alkaloids: Chemistry and Pharmacology*, 1988, **31**, A. Brossi, ed. Orlando: Academic Press.

10 J. M. Cassady, W. M. Baird, C. J. Chang, *J. Nat. Prod.*, 1990, **53**, 23–41.

11 F. Zunino, R. Gambetta, A. D. Marco, F. Zaccara, *Biochim. Biophys. Acta*, 1972, **277**, 489–498.

12 A. Marco, F. Arcamone, *Arzneim. Forsch.*, 1975, **25**, 368–374.

13 S. C. Pakrashi, P. Ghosh-Dastidar, S. Basu, B. Achari, *Phytochemistry*, 1977, **16**, 1103–1104.

14 B. Achari, S. Bandyopadhyay, A. K. Chakraborty, S. C. Pakrashi, *Org. Mag. Reson.*, 1984, **22**, 741-746.

15 J. B. Chaires, K. R. Fox, J. E. Herrera, M. Britt, M. J. Waring, *Biochemistry*, 1987, **26**, 8227–8236.

16 S. Chakraborty, R. Nandi, M. Maiti, B. Achari, C. R. Saha, S. C. Pakrashi, *Biochem. Pharmacol.*, 1989, **38**, 3683–3687.

17 S. Chakraborty, R. Nandi, M. Maiti, B. Achari, S. Bandyopadhyay, *Photochem. Photobiol.*, 1989, **50**, 685-689.

18 J. B. Chaires, *Biophys. Chem.*, 1990, **35**, 191–202.

19 S. Chakraborty, R. Nandi, M. Maiti, *Biochem. Pharmacol.*, 1990, **39**, 1181–1186.

20 R. Nandi, S. Chakraborty, M. Maiti, *Biochemistry*, 1991, **30**, 3715–3720.

21 M. Maiti, G. Suresh Kumar, *Med. Res. Rev.*, 2007, **27**, 649–695.

22 A. Das, K. Bhadra, B. Achari, P. Chakraborty, G. Suresh Kumar, *Biophys. Chem.*, 2011, **155**, 10–19.

23 A. Das, K. Bhadra, G. Suresh Kumar, *PLoS ONE,* 2011, **6,** e23186.

24 A. Das, G. Suresh Kumar, *J. Chem. Thermodyn.*, 2012, **54**, 421–428.

25 A. Das, G. Suresh Kumar, *Biochim. Biophys. Acta*, 2013, **1830**, 4708-4718.

26 C. Q. Jiang, M. X. Gao, X. Z. Meng, *Spectrochim. Acta, Part* A, 2003, **59**, 1605-1610.

27 K. Tang, Y. M. Qin, A. H. Lin, X. Hu, G. L. Zou, *J. Pharm. Biomed. Anal.*, 2005, **39**, 404–410.

28 H. A. Benesi, J. H. Hildebrand, *J. Am. Chem. Soc.*, 1949, **71**, 2703–2707.

29 J. R. Lakowicz, G. Weber, *Biochemistry*, 1973, **12**, 4171–4179.

30 H. Zhang, X. Huang, M. Zhang, *Mol. Biol. Rep.*, 2008, **35**, 699–705.

31 A. Y. Khan, M. Hossain, G. Suresh Kumar, *Chemosphere*, 2012, **87**, 775–781.

32 V. N. Uversky, N. V. Narizhneva, T. V. Ivanova, A. Y. Tomashevski, *Biochemistry*, 1997, **36**, 13638–13645.

33 D. Bose, D. Sarkar, N. Chattopadhyay, *Photochem. Photobiol.*, 2010, **86**, 538–544.

34 J. R. Lakowicz, *Principles of Fluorescence Spectroscopy,* Plenum Press, New York, 1983.

35 N. J. Buurma, I. Haq, *Methods*, 2007, **42**, 162–172.

36 A. L. Faig, *Biopolymers,* 2007, **87,** 293–301.

37 R. S. Spolar, M. T. Record Jr., *Science*, 1994, **263**, 777–784.

38 M. T. Record Jr., C. F. Anderson, T. M. Lohman, *Q. Rev. Biophys*. 1978, **11**, 103–178.

39 M. Hossain, A. Y. Khan, G. Suresh Kumar, *J. Chem. Thermodynamics,* 2012, **47**, 90–99.

40 A. Y. Khan, M. Hossain, G. Suresh Kumar, *Mol. Bio. Rep*. 2013, **40**, 553-566.

41 P. Giri, G. Suresh Kumar, *Biochim. Biophys. Acta*, 2007, **1770**, 1419-1426.

42 P. Giri, G. Suresh Kumar, *Arch. Biochem. Biophys*., 2008, **474**, 183-192.

43 K. Bhadra, M. Maiti, G. Suresh Kumar, *Biochim. Biophys.Acta*, 2007, **1770**, 1071–1080.

44 M. Hossain, A. Y. Khan, G. Suresh Kumar, *PLoS ONE,* 2011, **6**, e18333.

Figure captions

Fig. 1. Chemical structure of (A) aristololactam-β-D-glucoside and (B) daunomycin.

Fig. 2. Absorption spectral changes of (A) ADG (8 μM) treated with 0, 80, 160, 320, 560 and 800 μM (curves 1–6) of HSA and (B) DAN (8 μM) treated with 0, 16, 32, 64, 108, 128 and 160 μM (curves 1–7) of HSA. Inset: Respective Benesi-Hildebrand plots for the binding.

Fig. 3. Fluorescence spectral changes of HSA (1 μM) treated with (A) 0, 5, 10, 15, 20, 30, 40, 50, 70 and 90 μM of ADG (curves 1-10) and (B) 0, 2, 4, 6, 8, 10, 12, 16, 20 and 24 μM of DAN (curves 1-10). Stern-Volmer plots of (C) ADG and (D) DAN at 288.15 (■), 298.15 (●) and 308.15 K (▲), respectively.

Fig. 4. (A) Far UV circular dichroism spectral changes of HSA (1 μM) on interaction with 0, 0.2, 0.4, 0.8, 1.5, 2.0 μM of DAN (curve 1-6), (B) Near UV circular dichroism spectral changes of HSA (5 μM) on interaction with 0, 2, 4, 6, 8 and 10 μM of ADG (curves 1-6), and (C) Near UV circular dichroism spectral changes of HSA (5 μM) on interaction with 0, 2, 5, 7.5 and 10 μM of DAN (curves 1-5).

Fig. 5. Three-dimensional fluorescence spectra and contour maps of HSA (A, B), HSA-ADG complex (C, D) and HSA-DAN complex (E, F).

Fig. 6. Steady state fluorescence anisotropy change in (A) ADG and (B) DAN with increasing concentration of HSA. Inset: Decrease in the steady state fluorescence anisotropy of HSA-bound drugs against increasing urea concentration.

Fig. 7. ITC profiles for the binding of (A) ADG and (B) DAN to HSA at 298.15 K. Top panels present plots of enthalpy against time representing the raw data for the

sequential injection of HSA into the drug solutions and dilution of HSA into the buffer (curves off set). In the corresponding lower panels, plot of enthalpy against molar ratio showing the integrated heat results after correction of heat of dilution against the molar ratio of HSA/drug is presented. The data points (closed squares) were fitted to a one-site model and the solid lines represent the best-fit results.

Fig. 8. Plot of enthalpy against molar ratio showing the integrated heat results of (A) ADG and (B) DAN titration to HSA after correction of heat of dilution at 288.15 K (●), 298.15 K (▲) and 308.15 K (■), respectively. The results were fitted to a one-site model and the solid lines represent the best-fit data.

Fig. 9. Graph showing variation of the thermodynamic parameters with temperature for the binding of (A) ADG and (B) DAN to HSA.

Fig. 10. Non-polyelectrolytic (black) (ΔG^o_t) and polyelectrolytic (ΔG^o_{pe}) (shaded) contribution to the standard molar Gibbs energy for the binding of (A) ADG and (B) DAN to HSA.

Fig. 11. DSC thermograms of HSA (curve 1), HSA–ADG complex (curve 2) and HSA-DAN complex (curve 3).

Table 1 Stern–Volmer quenching constants (K_{sv}), static quenching constants (K_{LB}) and binding constant (K_b) and number of binding sites (n) for the interaction of ADG and DAN with HSA at different temperatures[a]

Drug	Temperature (K)	K_{sv} x 10^{-4} /M^{-1}	K_{LB} x 10^{-4} /M^{-1}	K_b x 10^{-4} /M^{-1}	n
ADG	288.15	3.90	4.46	4.57	1.09
	298.15	3.10	3.30	3.39	1.10
	303.15	2.46	2.33	2.24	1.12
DAN	288.15	22.4	20.5	20.8	1.12
	298.15	17.7	15.8	17.2	1.16
	303.15	13.0	11.4	11.9	1.17

[a]The data presented are averages of four determinations.

Table 2 Data derived from 3-D fluorescence of HSA, HSA-ADG and HSA-DAN complexes[a]

System	Peaks	Peak position $\lambda_{ex}/\lambda_{em}$ (nm/nm)	Stokes Shift	Intensity (F)
HSA	peak 1	280/350	70	445.50
	peak 2	230/350	120	421.20
HSA +ADG	peak 1	280/352	72	220.77
	peak 2	230/354	124	122.26
HSA +DAN	peak 1	280/347	67	122.80
	peak 2	230/346	116	63.47

REVISED MANUSCRIPT RA-ART-05-2014-004327

Table 3 Temperature dependent isothermal titration calorimetry data for the binding of ADG and DAN to HSA[a]

Drug	T (K)	K x 10^4 /M^{-1}	n	ΔH^o kcal/mol	$T\Delta S^o$ kcal/mol	ΔG^o kcal/mol	ΔC_p^o cal/mol /^{o}C
ADG	288.15	3.80	1.10	-1.80	4.27	-6.07	
	298.15	3.50	1.25	-2.80	3.44	-6.24	-86
	308.15	3.03	1.28	-3.52	2.84	-6.36	
DAN	288.15	28.0	1.01	-2.00	5.18	-7.18	
	298.15	19.5	1.13	-3.40	3.81	-7.22	-127
	308.15	14.3	1.56	-4.53	2.75	-7.28	

[a]All the data in this table are derived from ITC experiments conducted in CP buffer of 10 mM [Na$^+$], pH 7.2, and are averages of four determinations. K and ΔH^o values were determined from ITC profiles fitting to Origin 7 software as described in the text.

Table 4 Salt dependent isothermal titration calorimetry data for the binding of ADG and DAN to HSA[a]

Drug	$[Na^+]$	$K \times 10^4$ $/M^{-1}$	n	ΔH^o kcal /mol	$T\Delta S^o$ kcal/mol	ΔG^o kcal/mol	ΔG^o_{pe} kcal/mol	ΔG^o_t kcal/mol
ADG	10	3.50	1.25	-2.80	3.44	6.13	0.78	5.35
	20	3.05	1.30	-2.50	3.50	6.05	0.66	5.38
	50	2.20	1.45	-2.12	3.64	5.86	0.51	5.35
DAN	10	19.5	1.13	-3.40	3.81	7.14	1.35	5.79
	20	10.5	1.20	-3.20	3.57	6.77	1.15	5.63
	50	8.4	1.22	-2.85	3.96	6.64	0.88	5.77

[a]All the data in this table are derived from ITC experiments conducted in CP buffer of 10 mM $[Na^+]$, pH 7.2, and are averages of four determinations. K and ΔH^o values were determined from ITC profiles fitting to Origin 7 software as described in the text.

Fig. 1
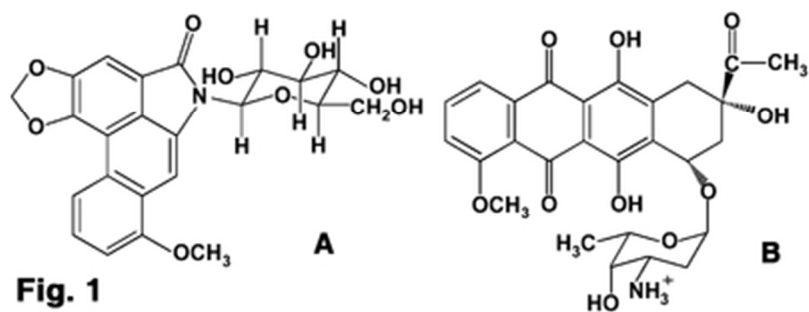
Chemical structure of (A) aristololactam-β-D-glucoside and (B) daunomycin.
34x12mm (300 x 300 DPI)
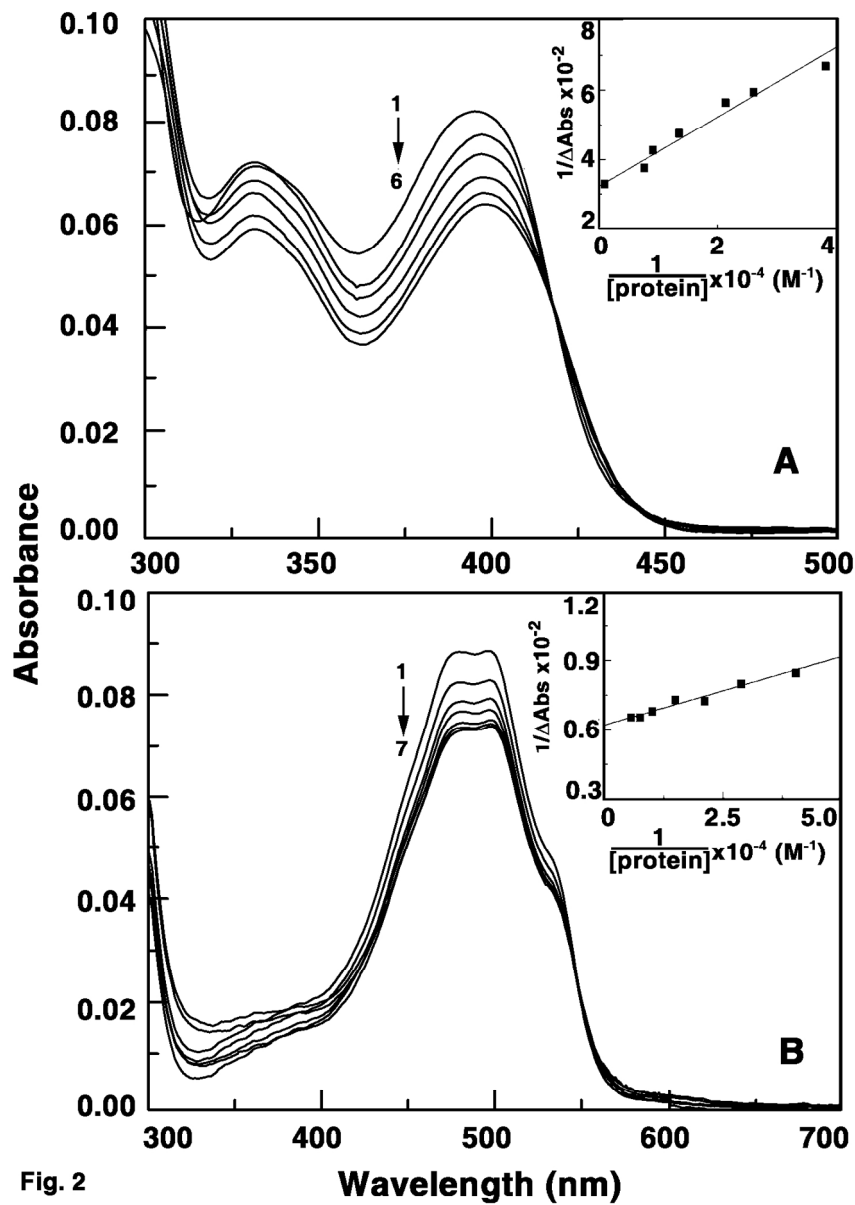
Fig. 2

Absorption spectral changes of (A) ADG (8 µM) treated with 0, 80, 160, 320, 560 and 800 µM (curves 1–6) of HSA and (B) DAN (8 µM) treated with 0, 16, 32, 64, 108, 128 and 160 µM (curves 1–7) of HSA. Inset: Respective Benesi-Hildebrand plots for the binding.
126x176mm (300 x 300 DPI)
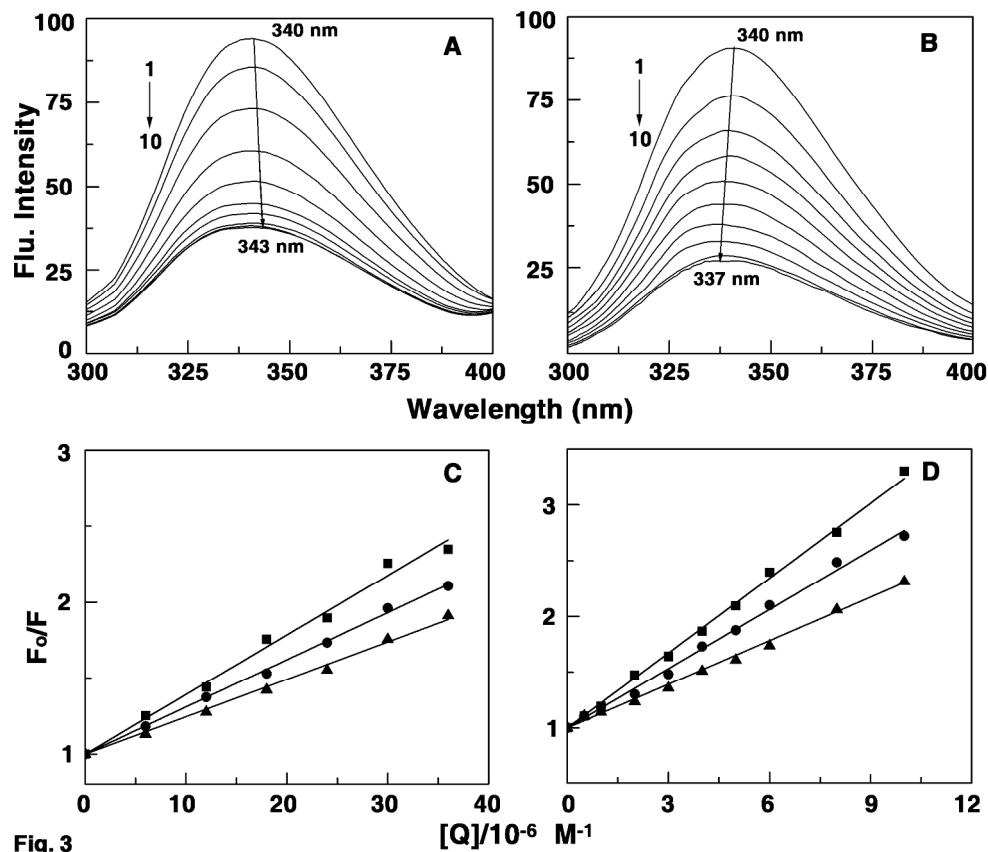
Fig. 3

Fluorescence spectral changes of HSA (1 µM) treated with (A) 0, 5, 10, 15, 20, 30, 40, 50, 70 and 90 µM of ADG (curves 1-10) and (B) 0, 2, 4, 6, 8, 10, 12, 16, 20 and 24 µM of DAN (curves 1-10). Stern-Volmer plots of (C) ADG and (D) DAN at 288.15 (closed square), 298.15 (closed circle) and 308.15 K (closed triangle), respectively.
209x183mm (300 x 300 DPI)
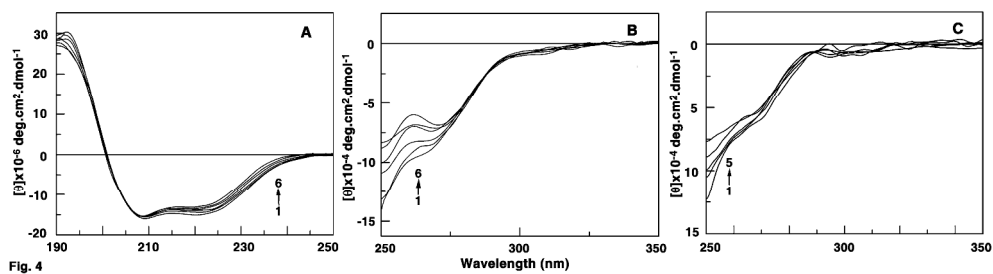
Fig. 4

(A) Far UV circular dichroism spectral changes of HSA (1 μM) on interaction with 0, 0.2, 0.4, 0.8, 1.5, 2.0 μM of DAN (curve 1-6), (B) Near UV circular dichroism spectral changes of HSA (5 μM) on interaction with 0, 2, 4, 6, 8 and 10 μM of ADG (curves 1-6), and (C) Near UV circular dichroism spectral changes of HSA (5 μM) on interaction with 0, 2, 5, 7.5 and 10 μM of DAN (curves 1-5).
378x107mm (300 x 300 DPI)
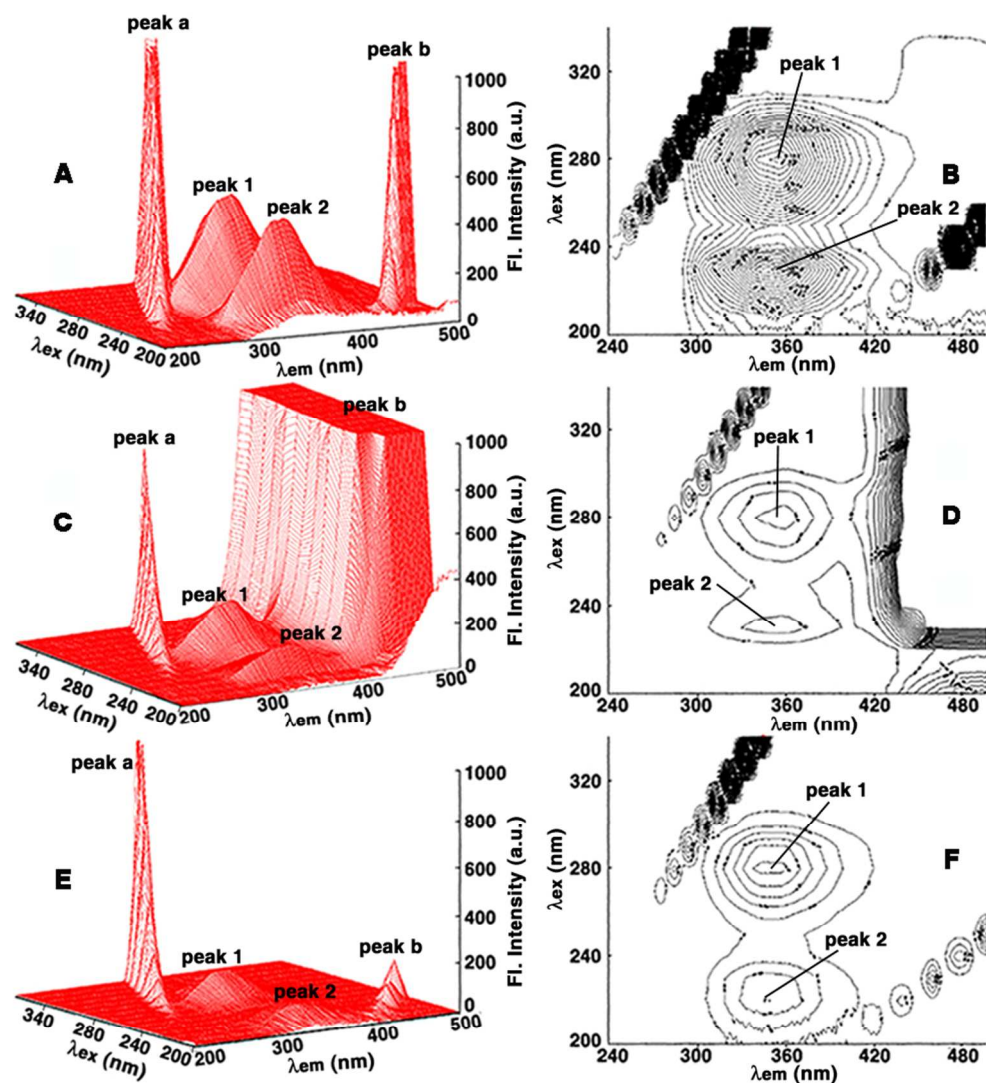
Fig. 5

Three-dimensional fluorescence spectra and contour maps of HSA (A, B), HSA-ADG complex (C, D) and HSA-DAN complex (E, F).
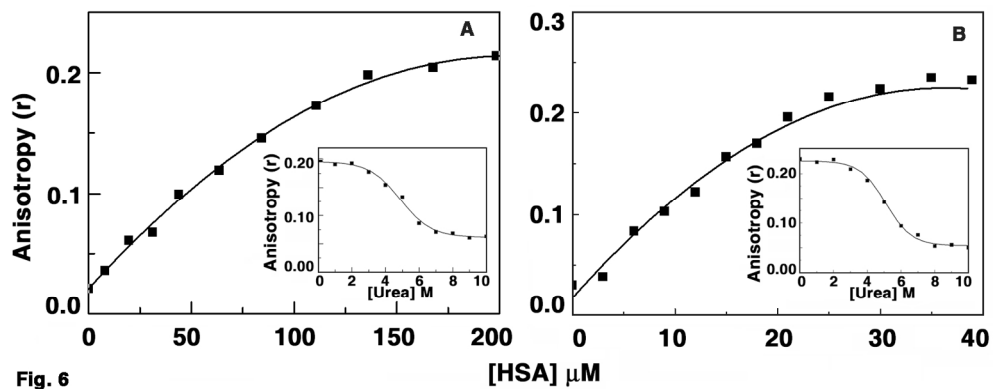
Fig. 6

Steady state fluorescence anisotropy change in (A) ADG and (B) DAN with increasing concentration of HSA. Inset: Decrease in the steady state fluorescence anisotropy of HSA-bound drugs against increasing urea concentration.
145x56mm (300 x 300 DPI)
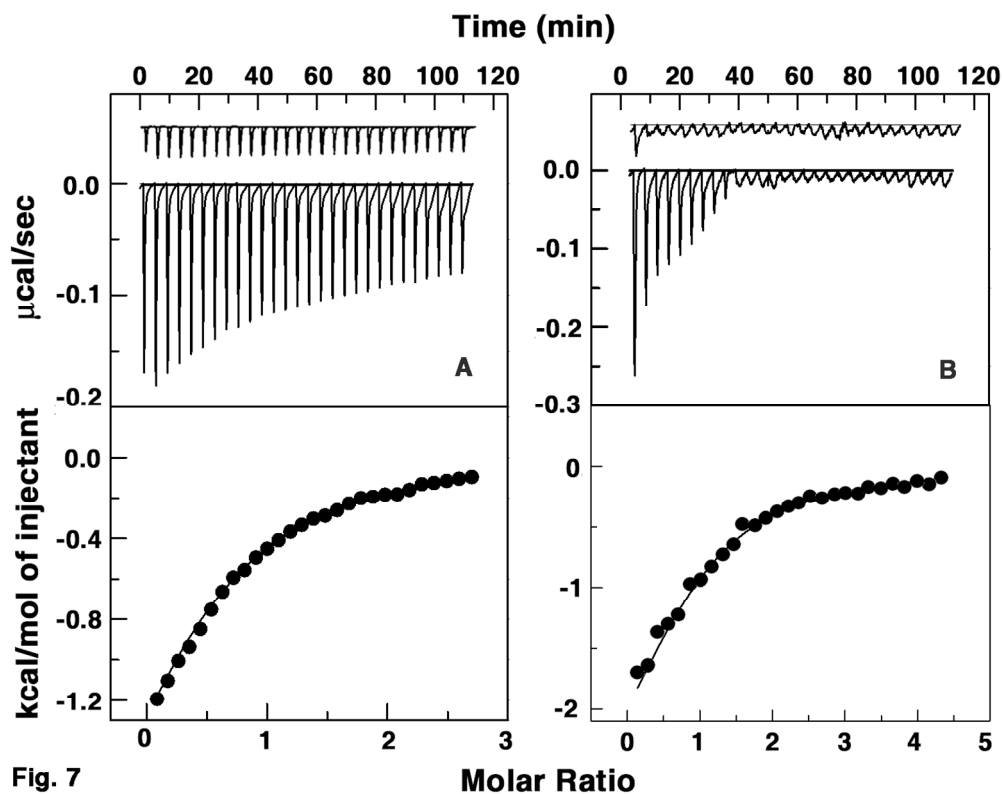
ITC profiles for the binding of (A) ADG and (B) DAN to HSA at 298.15 K. Top panels present plots of enthalpy against time representing the raw data for the sequential injection of HSA into the drug solutions and dilution of HSA into the buffer (curves off set). In the corresponding lower panels, plot of enthalpy against molar ratio showing the integrated heat results after correction of heat of dilution against the molar ratio of HSA/drug is presented. The data points (closed squares) were fitted to a one-site model and the solid lines represent the best-fit results.

126x98mm (300 x 300 DPI)
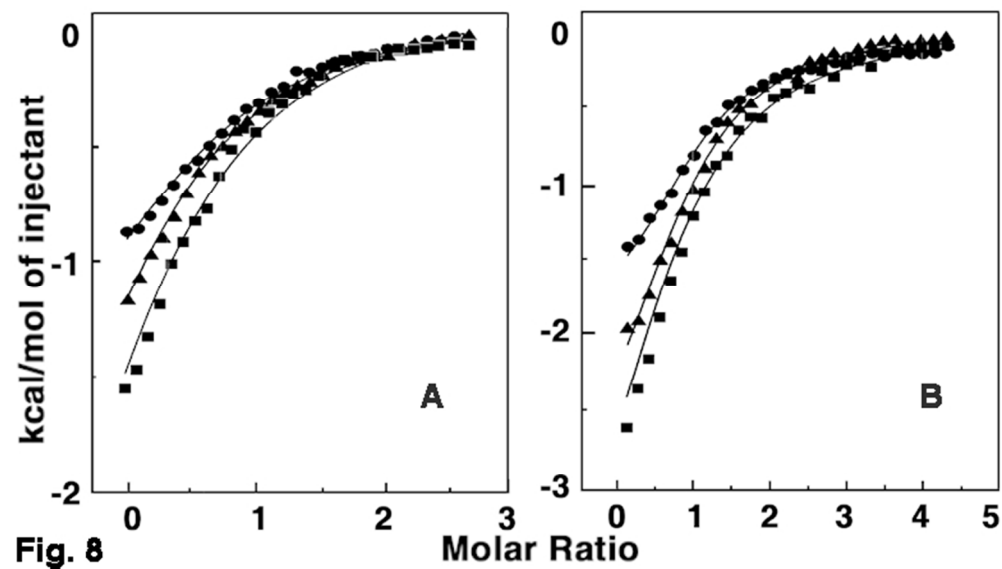
Fig. 8

Plot of enthalpy against molar ratio showing the integrated heat results of (A) ADG and (B) DAN titration to HSA after correction of heat of dilution at 288.15 K (●), 298.15 K (▲) and 308.15 K (■), respectively. The results were fitted to a one-site model and the solid lines represent the best-fit data.
66x37mm (300 x 300 DPI)
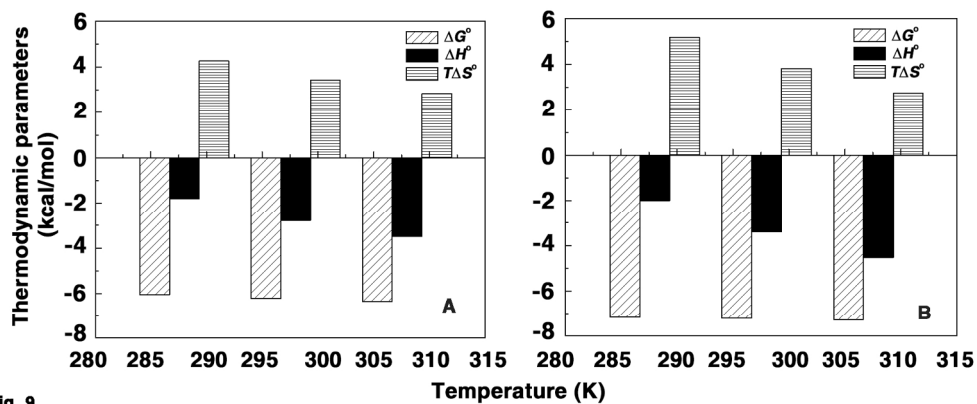
Fig. 9

Graph showing variation of the thermodynamic parameters with temperature for the binding of (A) ADG and (B) DAN to HSA.
164x67mm (300 x 300 DPI)
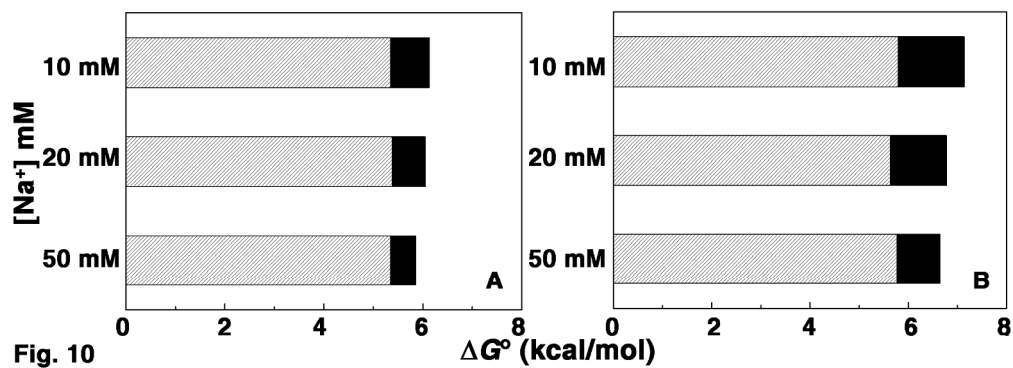
Fig. 10

Non-polyelectrolytic (black) (ΔGot) and polyelectrolytic (ΔGope) (shaded) contribution to the standard molar Gibbs energy for the binding of (A) ADG and (B) DAN to HSA.
205x74mm (300 x 300 DPI)

Fig. 11
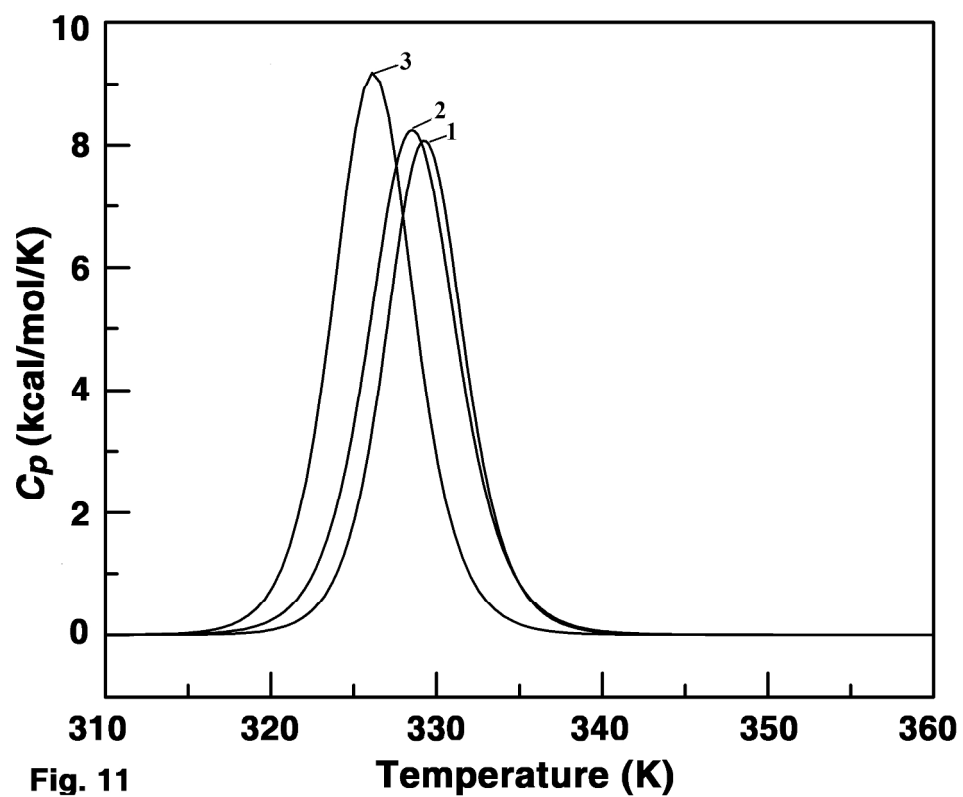
DSC thermograms of HSA (curve 1), HSA–ADG complex (curve 2) and HSA-DAN complex (curve 3).
230x189mm (300 x 300 DPI)

Binding studies of aristololactam- β-D-glucoside and daunomycin to human serum albumin

Abhi Das and Gopinatha Suresh Kumar*

Biophysical Chemistry Laboratory, Chemistry Division
CSIR-Indian Institute of Chemical Biology
Kolkata 700 032
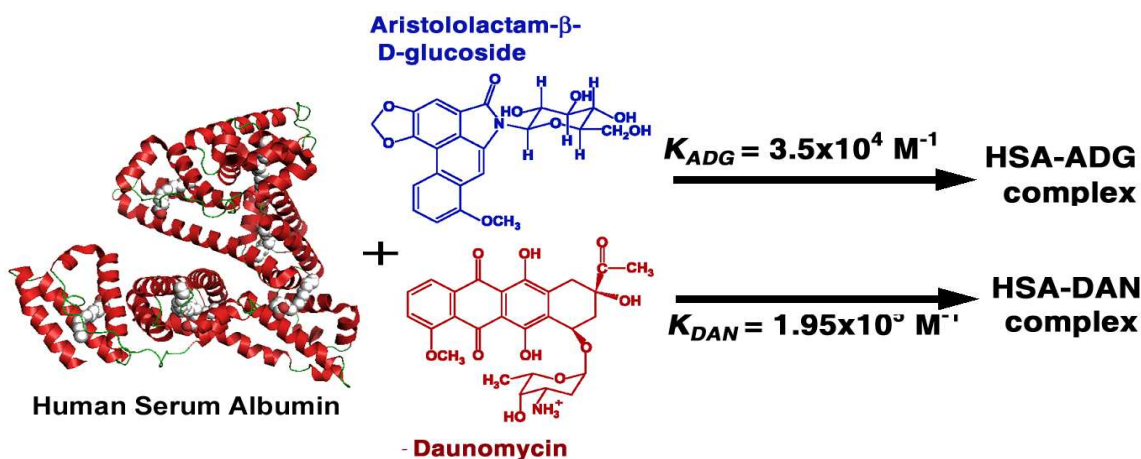
The binding of two carbohydrate containing molecules aristololactam-β-D-glucoside and daunomycin with human serum albumin was evaluated by biophysical techniques.